Supporting Information

Yawata et al. 10.1073/pnas.1318943111

SI Results and Discussion

Attachment to Chitin Beads. Our results showed that the difference in attachment between bulk-fluid and small-particle isolates (S population) and large-particle isolates (L population) is largely independent of the chemistry (hydrophobic vs. hydrophilic), physical state (crystalline, hydrogel), and biological state (presence/absence of an existing biofilm) of the solid-phase material (Fig. 1*A* and Fig. S1 *A*–*C* and *E*). One exception we encountered is chitin. Chitin is an abundant polymer in the ocean, and the chitin-attachment protein GbpA (1) is common among *Vibrionaceae*. A genome comparison revealed the conservation of a *gbpA* homolog in both the S and L populations, implying that specific attachment to chitin is not involved in their ecological differentiation. Indeed, our attachment assay showed comparable attachment to chitin particles by one S and one L group isolate (Fig. S1*C*), in agreement with the absence of known genetic differences related to chitin attachment. This result is further corroborated by a recent report of the absence of *Vibrio cyclitrophicus* on specimens of copepod (2), which possess chitinous exoskeleta.

Interaction Between Cells and Chemoattractant-Releasing Surfaces. Our analysis of bacterial behavior under changing nutrient conditions showed that both S and L isolates accumulated near the chemoattractant-releasing agarose sidewall (Fig. 3). The number of swimming cells decreased to nearly zero for isolate ZF270 (L population) and did not increase again after the gradient direction was reversed (Fig. 3*C*), which we interpreted as cells having attached to the chemoattractant-releasing agarose surface. In contrast, although the number of swimming 1F111 cells (S population) also initially decreased, it increased again after gradient reversal (Fig. 3*C*), allowing cells to migrate to the new source (opposite sidewall) and suggesting that 1F111 cells did not attach to the chemoattractant-releasing agarose surface.

Here we investigate in more detail the surface-interaction dynamics associated with the gradient reversal by means of a gradient generator (design 3; Fig. S5) where the primary gradient (vertical) is perpendicular to the plane of observation (horizontal). In particular, we positioned the imaging plane directly below the agarose ceiling of the test chamber, capturing cell trajectories over time. Results (Figs. S7 and S8) show that, shortly after injection of cells into the test channel, swimming cells appeared on the surface for both isolates (ZF270 and 1F111). However, 10 min after injection there were almost no swimming ZF270 cells (L population) (Figs. S7 and S8*A*) and the number of attached cells increased (Fig. S8*B*), together signifying that cells rapidly adhered to the surface. In contrast, at the same point in time the number of swimming 1F111 cells (S population) had increased considerably (Figs. S7 and S8*A*), as more cells swam toward the ceiling surface by chemotaxis and only small numbers of cells attached to the surface (Fig. S8*B*). This indicates that cells from the S-population isolate "hovered" at the surface, swimming in close proximity to it without attaching. Hovering cells left the surface when the direction of the gradient was reversed (Figs. S7 and S8*A*), further confirming the ability of S-population cells to rapidly pursue new nutrient opportunities.

Substrate Utilization. Our results showed that unspecific surface attachment and biofilm formation were consistent predictors of the preference for particles of the L population, suggesting that ecological differentiation between the two populations is mediated by differences in attachment rates to and residence times on particles. Here we consider whether another trait—metabolic preference—can be a key driver of ecological differentiation between the two populations. To this end, we analyzed substrate utilization using a Biolog assay. Results (Fig. S9) showed that both populations actively oxidize highly bioreactive carbon compounds, such as aldose sugars and protein-constituting amino acids, and neither population oxidized many compounds of lower bioreactivity (Fig. S9), supporting the idea that both populations exploit localized sources of highly bioreactive carbon compounds, such as marine particles (3–6). The lack of major differentiation in substrate utilization between the S and L populations, among the compounds tested, agrees with the finding that neither S- nor L-population isolates harbor any unique genes related to primary metabolism (7). Although identity in the metabolic preferences of S- and L-population isolates is exceedingly difficult to prove, both gene content and metabolic analyses suggest similarity between the two populations. Although metabolic activity could be differentially tuned in situ via differential gene-expression levels, these potential metabolic differences do not counter the proposed model, which, instead of metabolic differentiation, hinges on differentiation in the spatial behaviors of bacteria in response to the microscopic spatial structure of nutrients in their local environment.

SI Materials and Methods

Bacterial Isolates and Cell Culture. The isolates and plasmids used in this study are listed in Table S1. For routine culture, bacterial isolates were grown in 1/2 strength 2216 medium (8) or on 2216 agar plates at 30 °C. An orbital shaker (600 rpm) was used for liquid cultures. For culturing isolates harboring pGFP, spectinomycin (50 μg/mL) was added to maintain the plasmid. Unless otherwise stated, all assays were performed for each of the 12 strains listed in Table S1.

Fabrication and Operation of Microfluidic Devices. Polydimethylsiloxane (PDMS) channels were designed using CAD software (Autodesk) and printed onto transparency film with a high-resolution image setter (Fineline Imaging). Microchannels were fabricated by prototyping against a silicon master with positive-relief features using standard soft lithography techniques (9, 10). The PDMS layer was patterned with two or three parallel channels that were 20 mm-long, 100 μm-deep, and either 600 μm (design 1) or 1 mm (design 2)-wide. PDMS layers with embossed channels were obtained by molding against the silicon master, baking at 65 °C for 12 h, peeling off the hardened PDMS, cutting it to size, and punching inlets and outlets. Different configurations were used for the agarose layer. For design 1, we used a plain, 500 μm-thick agarose layer (Fig. S2*A*). For design 2, we used a 500 μm-thick agarose layer in which we carved a 20 mm-long, 1 mm-wide, 500 μm-deep trench spanning the entire thickness of the layer (Fig. S3*A*). In both cases, the agarose layer was made from a 3% (wt/vol) solution of agarose in filtered autoclaved seawater, heated in a microwave oven, injected into a mold with a plastic syringe, allowed to gel at room temperature, released from the mold, and used. For the mold, we used two stacked glass slides with a silicone gasket between them as an edge seal, and the thickness of the agarose slab was set by the thickness of the gasket. The trench (design 2) in the agarose layer was obtained by placing within the mold a 0.5 mm-thick, 1 mm-wide gasket strip before injecting the agarose.

The gradient generator was placed on an inverted microscope (Nikon; TE2000E). Flexible polyethylene tubing (Cole-Parmer;

inner/outer diameter 0.5/1.5 mm) was used to connect the inlets of the source and sink channels with two or three 3-mL plastic syringes (Becton Dickinson), driven by a syringe pump (Harvard Apparatus; PHD 2000) operated in "withdrawal" mode at 10 μL/min in all cases. After injection of the cell suspension, the inlet and outlet of the test channel were sealed using small PDMS blocks to prevent evaporation and residual flow in the channel.

Interaction Between Cells and Chemoattractant-Releasing Surfaces: Design 3. In addition to the two gradient generators used to generate the data presented in the main text (design 1, Fig. S2, results in Fig. 2; design 2, Fig. S3, results in Fig. 3), a third microfluidic gradient generator (design 3, Fig. S5, results in Figs. S7 and S8) was used to support results on cell attachment under temporally varying gradients. Design 3, also modified from ref. 11, is made of three layers: a PDMS layer on top (impermeable to solutes), an agarose layer in the middle (permeable to solutes), and a glass slide at the bottom (for support). The PDMS layer and agarose layer were fabricated using the same methods as in designs 1 and 2. The PDMS layer was patterned with three parallel channels that were 20 mm-long, 100 μm-deep, and 1 mm-wide. We used a 1 mm-thick agarose layer in which we carved a 35 mm-long, 1 mm-wide, 500 μm-deep groove (Fig. S5*A*). The groove in the agarose layer was obtained by placing within the mold a 0.5 mm-thick, 1 mm-wide gasket strip before injecting the agarose. Operation of the device also mirrored that of designs 1 and 2.

Design 3 (Fig. S5*A*) among the microfluidic gradient generators was used to study the interaction of bacteria with the surface-releasing chemoattractant in greater detail compared with what was possible using design 2, because design 3 creates a gradient of attractant in the vertical direction, namely perpendicular to the imaging plane (Fig. S5*B*). As in design 2, the test channel was located within the agarose layer, but the PDMS layer now contained three irrigation channels. Flowing chemoattractant in the central irrigation channel and filtered autoclaved seawater in the two side irrigation channels resulted in a chemoattractant gradient with a strong vertical component across the agarose layer directly above the test channel. Consequently, a vertical chemoattractant gradient formed within the test channel by diffusion of the chemoattractant into the test channel from its top surface (Fig. S5*B*). After >10 min from the start of the irrigation, mid–exponential-phase cells (OD_{600} 0.4) were diluted to OD_{600} 0.04 with filtered autoclaved seawater and injected into the test channel. The vertical gradient attracted cells toward the agarose ceiling of the test channel, where cell concentration and cell behavior could be imaged at high resolution in a horizontal plane directly underneath the ceiling. Furthermore, cell attachment to the ceiling surface was visualized by epifluorescence microscopy (as described above). Epifluorescence images were analyzed using ImageJ (National Institutes of Health) to enumerate attached cells. To assay the response to a temporal change in nutrient conditions, 10 min after injecting cells into the test channel, we reversed the direction of the chemoattractant gradient by swapping the irrigation of chemoattractant and filtered autoclaved seawater. Fig. S6 shows the results of a numerical model (see below) of the time course of the chemoattractant concentration field in the agarose layer and the test channel. Experiments were performed with two isolates (1F111-pGFP and ZF270-pGFP), with three independent experiments per isolate (Figs. S7 and S8).

Numerical Model. The time evolution of the concentration field of chemoattractant, $C(x,z)$, in a vertical cross-section (xz) of each gradient generator device (Figs. S3 and S5) was obtained by solving the diffusion equation in a 2D domain comprising the agarose layer and the test channel with COMSOL Multiphysics (v. 4.1). We modeled the continuous flow in the source and sink channels as time-varying boundary conditions applied at the interface between flowing fluid and the agarose layer. We used a diffusion coefficient of the chemoattractant, $D = 8.8 \times 10^{-8}$ m^2/s, both in agarose and in water (11). Interfaces other than agarose–fluid were modeled as no-flux boundary conditions.

To capture sudden changes in the chemoattractant concentration in the source and sink channels (e.g., at $t = 20$ min in Figs. S4 and S6), we used a smoothed step function. To model the injection of cells into the test channel associated with the complete replacement of the fluid in the test channel with new fluid at zero chemoattractant concentration (e.g., at $t = 10$ min in Fig. 3), we split each simulation into two parts: one running from $t = 0$ to 10 min and the second running from $t = 10$ to 40 min. For the first part, we used an initial condition $C(x,z) = 0$, whereas for the second part, we used as an initial condition the $C(x,z)$ field obtained at $t = 10$ min from the first part for the agarose layer and $C(x,z) = 0$ for the test channel. The domain was discretized in a dense mesh of at least 15,000 triangular elements, and simulations were run with a time step of 1 s.

Swimming-Speed Measurements. Late–exponential-phase cells (OD_{600} 0.8) were harvested, washed with filtered autoclaved seawater, and introduced into circular microchambers (5 mm diameter, 100 μm height) made of PDMS. The microchambers were placed on an inverted microscope (Nikon; TE2000E), and video microscopy and image analysis were used to track cells and obtain their swimming speed as described previously (12, 13). Briefly, cells were imaged in phase contrast using a 20× objective (N.A. 0.45) by acquiring sequences of 200 frames (movies) at 50 frames per s with a CCD camera (Cooke; PCO 1600). A particle-tracking software developed in-house (BacTrack) was used to determine bacterial trajectories and calculate mean swimming speeds (14). The swimming speed was determined as the mean over all motile cells and represents a 2D projection of the 3D swimming speed. Time-course measurements of speed as a function of growth time were performed for isolates 1F53 and ZF270 by sampling small aliquots from liquid cultures. Triplicate measurements were performed in all cases.

Surface Attachment. A mid–exponential-phase cell culture (OD_{600} 0.5) was washed with filtered autoclaved seawater, diluted to OD_{600} 0.005 (1.5×10^6 CFU/mL), and then a 1-mL aliquot was inoculated in a 35 mm-diameter Petri dish and incubated at 30 °C for 1 h. After removing planktonic cells by gently washing twice with filtered autoclaved seawater, images of the bottom of the Petri dish at three locations were taken by phase–contrast microscopy using a CCD camera (Cooke; PCO 1600). Surface attachment was quantified by counting the enumerating attached cells using ImageJ. Three independent cultures were assayed for each isolate.

To test for attachment to surfaces of different hydrophobicity (Fig. S1*A*), we used nontreated (contact angle 79.1 ± 4.8°) and plasma-treated (contact angle 46.1 ± 3.7°) 35 mm-diameter polystyrene Petri dishes. To obtain polystyrene surfaces with an even lower contact angle (28.5 ± 3.6°), additional plasma treatment was performed (Electro-Technic Products; BD-20). Surface contact angles were measured by photography and image analysis.

To test the attachment to agarose (Fig. S1*B*), the bottom of a Petri dish was covered with agarose [3% (wt/vol)]. To test the attachment to cellulose (Fig. S1*B*), cellulose chromatography paper (Whatman) was placed at the bottom of a Petri dish. A mid–exponential-phase cell culture (OD_{600} 0.5) was washed with fresh medium, diluted to OD_{600} 0.01 (3.0×10^6 CFU/mL), and then a 2-mL aliquot was introduced into the Petri dish. For the attachment assay with cellulose, GFP-expressing cells were used and visualized by epifluorescence microscopy (with the same illumination described above), because the opaque nature of cellulose hindered light microscopy. Two isolates expressing GFP

(1F111-pGFP and ZF270-pGFP) were used for attachment assays with cellulose, and the two wild-type isolates (1F53 and ZF270) were used for attachment to all other surfaces. Triplicate measurements were performed in all cases.

To test for attachment to chitin and alginate (Fig. S1*C*), a mid–exponential-phase cell culture (OD_{600} 0.5) was washed with fresh medium, diluted to OD_{600} 0.01 (3.0×10^6 CFU/mL), and then a 1-mL aliquot was introduced into a Petri dish containing chitin beads (New England Biolabs) or alginate beads (prepared as described below) and incubated at 30 °C for 1 h. Planktonic cells were removed by gently washing twice with filtered autoclaved seawater for several seconds. Wild-type cells (1F53 and ZF270) were stained with a fluorescent dye (Syto9; Life Technologies). Cells attaching on a bead were imaged with confocal microscopy using an LSM510 laser scanning microscope (Carl Zeiss) equipped with a 40× objective (N.A. 0.6; Plan-Neofluar). Cells were illuminated by a 488-nm argon laser and detected using a 505-nm long-pass filter. Attached cells were then enumerated using ImageJ. Twenty-five (alginate) or 10 (chitin) particles were counted for each isolate.

Preparation of Alginate Beads. Unless otherwise indicated, all reagents were obtained from Sigma. For production of alginate microparticles, we used a protocol modified from Poncelet et al. (15). Briefly, a sodium alginate solution (Sigma; A2158) at 2% (wt/vol) was prepared with Milli-Q water (Millipore) by stirring until complete dissolution. NaOH (0.1 M) was added to adjust the pH of the alginate solution to 7.6. A calcium carbonate nanoparticle suspension in Milli-Q water was added to achieve a final concentration of 50 mM calcium carbonate. The suspension was degassed and stored at 4 °C until further use. A detergent oil solution was prepared by dissolving detergents in mineral oil at concentrations of 4.5% (vol/vol) Span, 0.4% Tween, and 0.05% Triton. One hundred milliliters of the detergent oil solution was stirred at 200 rpm, and 20 mL of sodium alginate, calcium carbonate suspension was slowly added. Stirring continued at 200 rpm for 15 min to create the emulsion of alginate, calcium carbonate droplets in oil. The stirring rate was increased to 350 rpm, followed by the slow addition of 20 mL of solution of mineral oil with 80 μL of glacial acetic acid at a rate of 0.5 mL/min. Stirring continued for 1 h at 350 rpm. The microparticles that formed were extracted into 150 mL of 50 mM calcium carbonate and separated by decanting the supernatant. The microparticles were washed with 50 mM calcium carbonate until the supernatant remained clear. The microparticles were extracted several times with water-saturated ether to remove residual oil. The microparticles were resuspended in Milli-Q water and filtered through 300- and 65-μm filters to obtain an intermediate size fraction. The microparticles were washed with Milli-Q water and stored in 20% ethanol at 4 °C until further use.

Early-Stage Biofilm Formation. An overnight cell culture was washed with 1/2 strength 2216 medium, diluted to OD_{600} 0.005 (1.5×10^6 CFU/mL), and then a 1-mL aliquot was inoculated in an untreated, 35 mm-diameter polystyrene Petri dish and grown at 30 °C for 5 h. After removing planktonic cells by gently washing twice with fresh 2216 medium, images of the bottom of the Petri dish at three locations were taken by phase–contrast microscopy using a CCD camera (Cooke; PCO 1600). Early-stage biofilm formation was quantified by measuring the percentage of the surface area covered by cells using ImageJ. The time course of surface coverage was measured for two isolates (1F53 and ZF270) by sacrificing cultures at each time point. Triplicate measurements were performed for each isolate.

Late-Stage Biofilm Formation and Confocal Microscopy. To quantify later-stage biofilm formation, a mid–exponential-phase culture (OD_{600} 0.5) was diluted to OD_{600} 0.005 (1.5×10^6 CFU/mL) with 1/20 strength 2216 medium and injected to fill a 20 mm-long, 100 μm-high, 600 μm-wide microfluidic channel made of PDMS. After 30 min of no-flow conditions, which allowed initial cell attachment, a 2 μL/min flow of 1/20 strength 2216 medium was initiated and maintained for 72 h (3 d) using a syringe pump (PHD 2000; Harvard Apparatus) to supply attached cells with nutrients. Experiments were conducted at room temperature. Biofilms of cells expressing GFP and wild-type cells were imaged with epifluorescence confocal microscopy and confocal reflection microscopy, respectively. A Carl Zeiss LSM510 laser scanning microscope equipped with a 40× objective (N.A. 0.6; Plan-Neofluar) was used to acquire confocal microscopic images. For visualization of cells expressing GFP, cells were illuminated by a 488-nm argon laser and detected with a 505-nm long-pass filter. The biofilm thickness of GFP-expressing cells was quantified by analyzing images using COMSTAT (16) under MATLAB (The MathWorks). For visualization of the polysaccharide matrix (Fig. S1*D*), biofilms were stained with FITC-labeled lectin made from *Triticum vulgaris* (Sigma-Aldrich). FITC fluorescence was detected using the same light path as GFP. Confocal reflection microscopy (17) was used as an independent, non–fluorescence-based method to nondestructively acquire 3D images of biofilms. Biofilms were illuminated with a 633-nm helium-neon laser, and reflected light was collected through a 505-nm long-pass filter. Z-stack images were converted to a 3D projection (Fig. 1*C* and Fig. S1 *D* and *E*) by using LSM510 software (Carl Zeiss). Three independent cultures were assayed for each case.

Cell Attachment to Biofilms. To test for cell attachment to an established biofilm (Fig. S1*E*), a 3-d-old biofilm of wild-type isolate ZF270 (nonfluorescent) was prepared in a microchannel as described above. Then, GFP-expressing cells (1F111-pGFP and ZF270-pGFP), grown to mid-exponential phase, washed with filtered autoclaved seawater, and diluted to OD_{600} 0.04 (1.2×10^7 CFU/mL), were introduced into the microchannel by flowing a cell suspension at 100 μL/min for 3 min and incubated for 1 h at room temperature. Channels were subsequently washed with filtered autoclaved seawater for 3 min at 100 μL/min to remove planktonic cells. Finally, biofilms were visualized by confocal reflection microscopy, and GFP-expressing cells attaching to the (nonfluorescent) biofilm were imaged by epifluorescence confocal microscopy, as described above. The number of GFP-expressing cells in each optical slice was quantified with ImageJ. Triplicate experiments were performed for each isolate.

Comparison of Genetic and Phenotypic Information. The unrooted phylogenetic tree of the 12 isolates was generated based on the *hsp60* gene sequence (7) using the neighbor-joining method. The color map, showing the strength of phenotypes of individual isolates relative to the strongest measurement for each phenotype (100%), was generated using MATLAB. Data of swimming speed (μm/s) (Fig. 2*A*), chemotaxis strength (Fig. 2*D*), number of cells attaching on the polystyrene surface (cells per mm^2) (Fig. 1*A*), and area surface coverage (%) (Fig. 1*B*) were used to compare swimming-speed, chemotaxis, surface-attachment, and early-stage biofilm-formation phenotypes, respectively.

Substrate Utilization. Biolog GN2 plates were used to determine patterns of sole carbon source utilization for six representative isolates (results in Fig. S9), as previously described (18). Briefly, Biolog GN2 plates are microtiter plates in which each well contains an individual carbon source. Ninety-five carbon sources were tested in triplicate. Each well also contains an oxidation indicator (redox tetrazolium), which turns purple when substrates are used (oxidized). Cells were grown as a lawn on tryptic soy broth plus 1% salt and swabbed into marine inoculating media containing 25 mg/mL NaCl, 8 mg/mL $MgCl_2$, and 0.5 mg/mL KCl to an OD_{600} of 0.1. A 150-μL aliquot was inoculated in each well, and

plates were incubated for 4 d at 22 °C. Color development was evaluated by measuring the OD_{588} of each well with a Varioskan Flash Spectral Scanning Multimode Reader (Thermo Scientific). An average of three wells was assayed for each substrate.

Electron Microscopy. A mid–exponential-phase cell culture (OD_{600} 0.4) was gently washed twice with fresh filtered autoclaved seawater and placed on carbon-coated formvar grids (200 mesh), which were then negatively stained with 2% aqueous uranyl acetate for 1 min, rinsed, and imaged using a Tecnai Spirit transmission electron microscope (FEI) with an AMT CCD camera at 80 kV. The percentage of cells with pili and the average number of pili per cell were calculated from transmission electron microscopy images of 25 cells per isolate. Contrast enhancement, for the sole purpose of illustrating pili (Fig. 1*E*), was done with Photoshop CS5 (Adobe).

1. Kirn TJ, Jude BA, Taylor RK (2005) A colonization factor links *Vibrio cholerae* environmental survival and human infection. *Nature* 438(7069):863–866.
2. Preheim SP, Timberlake S, Polz MF (2011) Merging taxonomy with ecological population prediction in a case study of *Vibrionaceae*. *Appl Environ Microbiol* 77(20): 7195–7206.
3. Blackburn N, Fenchel T, Mitchell J (1998) Microscale nutrient patches in planktonic habitats shown by chemotactic bacteria. *Science* 282(5397):2254–2256.
4. Bell W, Mitchell R (1972) Chemotactic and growth responses of marine bacteria to algal extracellular products. *Biol Bull* 143(2):265–277.
5. Kirchman DL, Suzuki Y, Garside C, Ducklow HW (1991) High turnover rates of dissolved organic-carbon during a spring phytoplankton bloom. *Nature* 352(6336): 612–614.
6. Hama T, Yanagi K (2001) Production and neutral aldose composition of dissolved carbohydrates excreted by natural marine phytoplankton populations. *Limnol Oceanogr* 46(8):1945–1955.
7. Shapiro BJ, et al. (2012) Population genomics of early events in the ecological differentiation of bacteria. *Science* 336(6077):48–51.
8. ZoBell CE (1941) Studies on marine bacteria. I. The cultural requirements of heterotrophic aerobes. *J Mar Res* 4:42–75.
9. Whitesides GM, Ostuni E, Takayama S, Jiang XY, Ingber DE (2001) Soft lithography in biology and biochemistry. *Annu Rev Biomed Eng* 3:335–373.
10. Marcos SR (2006) Microorganisms in vortices: A microfluidic setup. *Limnol Oceanogr Methods* 4:392–398.
11. Ahmed T, Shimizu TS, Stocker R (2010) Bacterial chemotaxis in linear and nonlinear steady microfluidic gradients. *Nano Lett* 10(9):3379–3385.
12. Marcos, Fu HC, Powers TR, Stocker R (2012) Bacterial rheotaxis. *Proc Natl Acad Sci USA* 109(13):4780–4785.
13. Seymour JR, Simó R, Ahmed T, Stocker R (2010) Chemoattraction to dimethylsulfoniopropionate throughout the marine microbial food web. *Science* 329(5989): 342–345.
14. Stocker R, Seymour JR, Samadani A, Hunt DE, Polz MF (2008) Rapid chemotactic response enables marine bacteria to exploit ephemeral microscale nutrient patches. *Proc Natl Acad Sci USA* 105(11):4209–4214.
15. Poncelet D, et al. (1992) Production of alginate beads by emulsification/internal gelation. I. Methodology. *Appl Microbiol Biotechnol* 38(1):39–45.
16. Heydorn A, et al. (2000) Quantification of biofilm structures by the novel computer program COMSTAT. *Microbiology* 146(Pt 10):2395–2407.
17. Yawata Y, Nomura N, Uchiyama H (2008) Development of a novel biofilm continuous culture method for simultaneous assessment of architecture and gaseous metabolite production. *Appl Environ Microbiol* 74(17):5429–5435.
18. Konopka A, Oliver L, Turco RFJ, Jr. (1998) The use of carbon substrate utilization patterns in environmental and ecological microbiology. *Microb Ecol* 35(2):103–115.

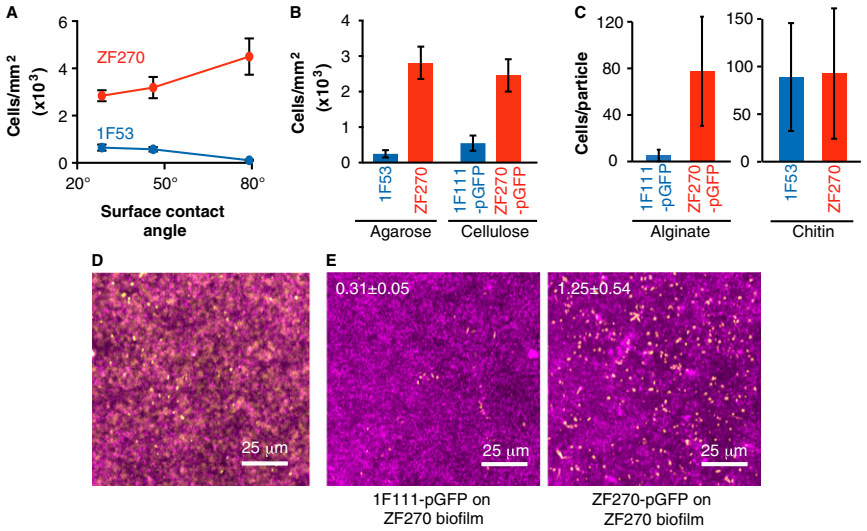

Fig. S1. Attachment of S and L isolates to various materials and biofilm formation. (*A*) Attachment to polystyrene surfaces with different contact angles, for one S (blue) and one L (red) isolate. Data are averages of three independent experiments, and error bars are SDs. (*B*) Attachment to agarose and cellulose surfaces after 1 h by one S (blue) and one L (red) isolate. Data are averages of three independent experiments, and error bars are SDs. (*C*) Attachment to alginate and chitin particles after 1 h for one S (blue) and one L (red) isolate. The *y* axis denotes attached cells per particle enumerated with confocal microscopy. Particles had a diameter of 65–300 μm. Data are averages of 25 (alginate) or 10 (chitin) particles, and error bars are SDs. (*D*) Extracellular polysaccharide matrix, stained with FITC-labeled lectin (yellow), in a 3-d-old L isolate (ZF270; purple) biofilm. (*E*) Attachment of GFP-tagged S and L cells (yellow) onto a previously established L-population biofilm (purple). Numbers in the top left of each panel denote attached cells per unit surface area (×10,000; mean ± SD; $n = 3$).

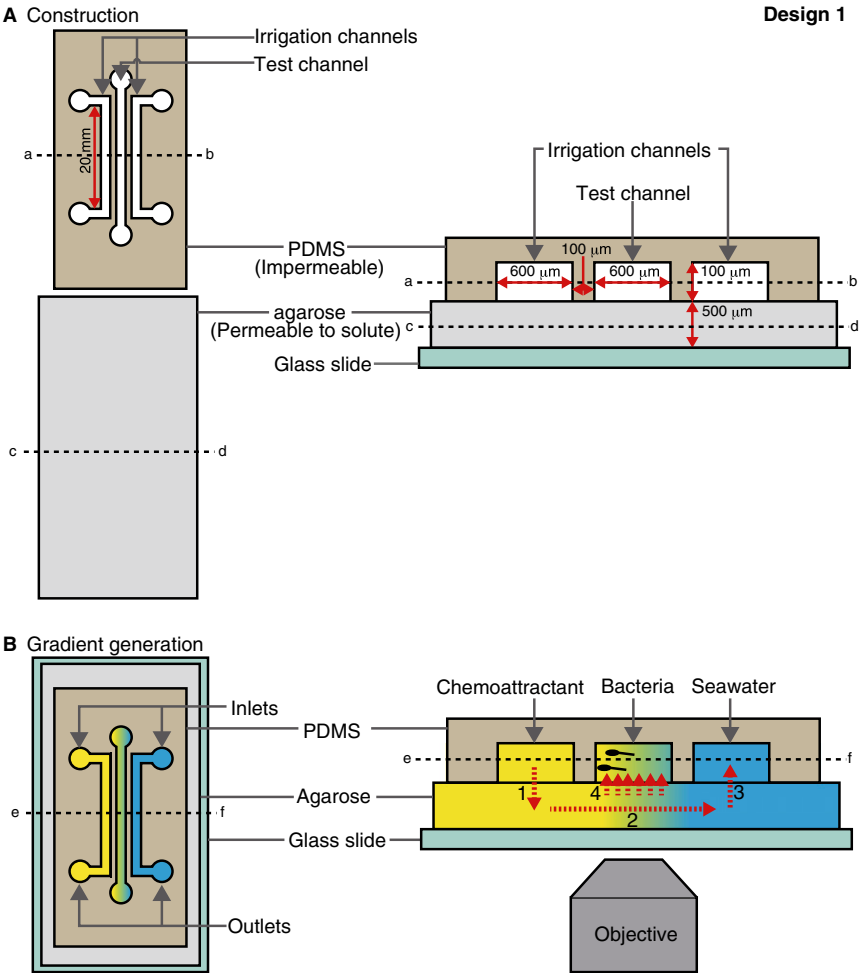

Fig. S2. Schematic of the design 1 gradient generator used to assay chemotaxis in steady, linear chemoattractant profiles. (*A*) Schematic of the cross-section of the assembled device (*Right*) and top view of each layer (*Left*). The top layer is made of PDMS, which is impermeable to solutes. The middle layer is made of agarose, which allows for the diffusion of chemoattractant used to establish the linear concentration profile. The bottom layer is a glass slide, used for support. Solid red arrows denote dimensions. (*B*) Schematic of the gradient-generation mechanism. The continuous flow of chemoattractant (yellow) and filtered autoclaved seawater (blue) within the two irrigation channels in the PDMS layer mediates the formation of a horizontal gradient (yellow-blue shading) in the underlying agarose layer and therefore in the test channel. Dashed red arrows in the cross-sectional view (*Right*) denote the different steps in the diffusion of the chemoattractant: Chemoattractant enters the agarose layer from the source irrigation channel (arrow 1), diffuses through the agarose layer (arrow 2), and is removed by diffusion into the sink irrigation channel (arrow 3), establishing a steady, linear, horizontal concentration profile across the agarose layer and therefore, by diffusion (arrow 4), also in the test channel. This design allows quantification of the bacterial swimming response to the steady chemoattractant gradient within the test channel (e.g., Fig. 2 *B–E*).

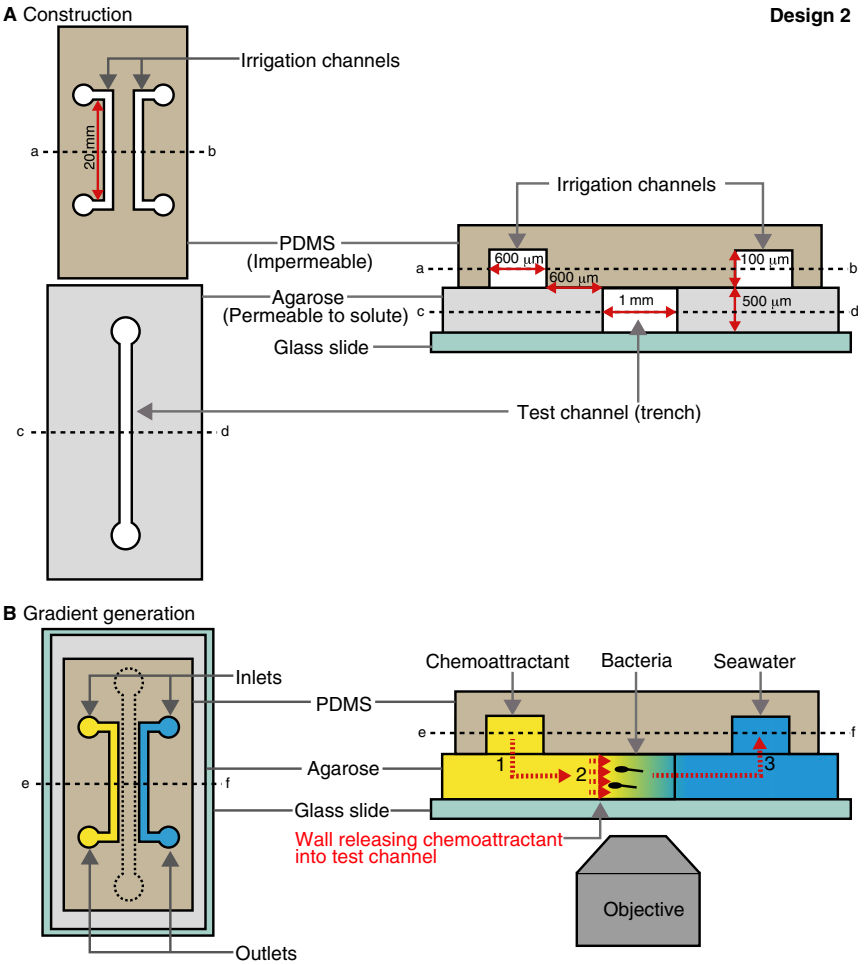

Fig. S3. Schematic of the design 2 gradient generator used to determine bacterial behavior under time-varying nutrient conditions. (*A*) Schematic of the cross-section of the assembled device (*Right*) and top view of each layer (*Left*). The top layer is made of PDMS, which is impermeable to solutes. The middle layer is made of agarose, which allows for the diffusion of chemoattractant used to establish the linear concentration profile. The test channel in this design is a "trench" spanning the entire thickness (500 μm) of the agarose layer. The bottom layer is a glass slide, used for support. Solid red arrows denote dimensions. (*B*) Schematic of the gradient-generation mechanism. The continuous flow of chemoattractant (yellow) and filtered autoclaved seawater (blue) within the two irrigation channels in the PDMS layer mediates the formation of a horizontal gradient (yellow-blue shading) in the underlying agarose layer and therefore in the test channel. Dashed red arrows in the cross-sectional view (*Right*) denote the different steps in the diffusion of the chemoattractant: Chemoattractant enters the agarose layer from the source irrigation channel (arrow 1), diffuses through the agarose layer and thus into the trench test channel (arrow 2), and is removed by diffusion into the sink irrigation channel (arrow 3). This design allows quantification of both the bacterial swimming response to the chemoattractant gradient and their attachment behavior at the agarose sidewall (e.g., Fig. 3).

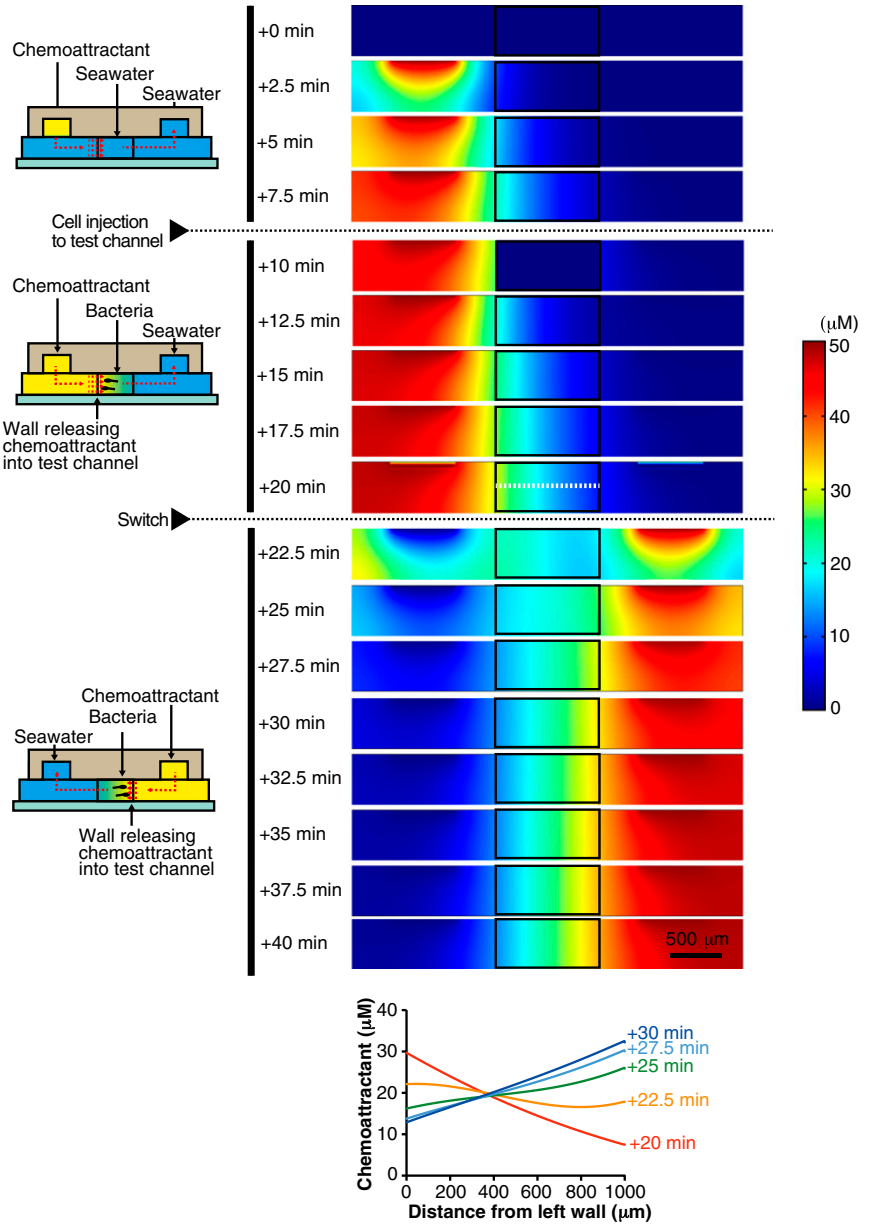

Fig. S4. Temporal evolution of the chemoattractant gradient in the design 2 microdevice (Fig. S3), modeled numerically. Colors represent the chemoattractant concentration (color map) within the agarose layer. Black boxes identify the test channel within the agarose layer in all panels. Different rows correspond to different times, as indicated by the labels on the left. For the first 20 min, the left irrigation channel carried 50 μM chemoattractant and the right irrigation channel carried seawater (0 μM). At 10 min past the initiation of gradient generation, cells were introduced into the test channel. After 20 min, the conditions were swapped: The left irrigation channel carried seawater (0 μM) and the right irrigation channel carried 50 μM chemoattractant. This resulted in rapid reversal of the chemoattractant gradient. (*Lower*) Temporal evolution of the chemoattractant concentration profile along the horizontal midline of the test channel (shown as a white dotted line in one of the panels).

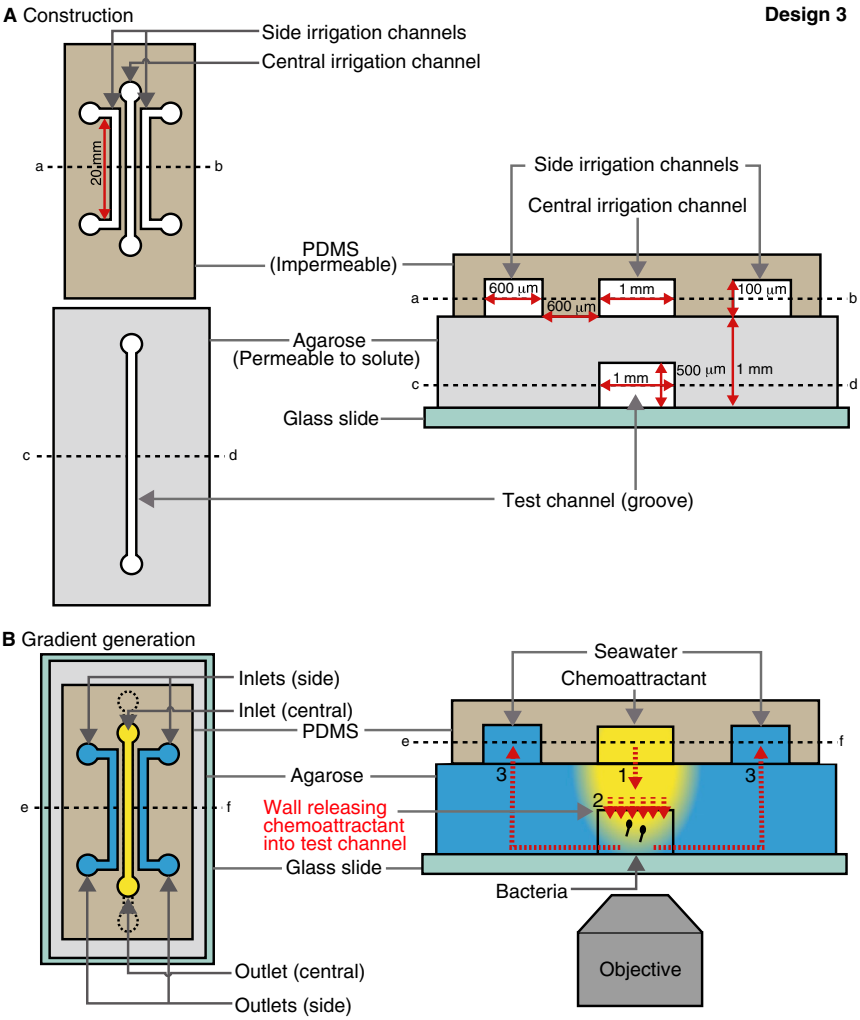

Fig. S5. Schematic of the design 3 gradient generator used to quantify the interaction between cells and chemoattractant-releasing surfaces. (*A*) Schematic of the cross-section of the assembled device (*Right*) and top view of each layer (*Left*). The top layer is made of PDMS, which is impermeable to solutes. The middle layer is made of agarose, which allows for the diffusion of chemoattractant used to establish the linear concentration profile. The test channel in this design is a "groove" with a depth (500 μm) equal to half the thickness of the agarose layer (1 mm). The bottom layer is a glass slide, used for support. Solid red arrows denote dimensions. (*B*) Schematic of the gradient-generation mechanism. The continuous flow of chemoattractant (yellow) in the central irrigation channel and of filtered autoclaved seawater (blue) in the two side irrigation channels within the PDMS layer mediates the formation of a gradient (yellow-blue shading) with a strong vertical component within the agarose layer and thus inside the test channel. Dashed red arrows in the cross-sectional view (*Right*) denote the different steps in the diffusion of the chemoattractant: Chemoattractant enters the agarose layer from the central irrigation channel (arrow 1), from where it enters the test channel through the test channel's ceiling (arrow 2), finally leaving primarily from the test channel's sidewalls and diffusing into the side irrigation channels (arrows 3). This design allows a detailed quantification of bacteria interacting with the horizontal ceiling surface of the test channel as a result of the vertical chemoattractant gradient (e.g., Figs. S7 and S8).

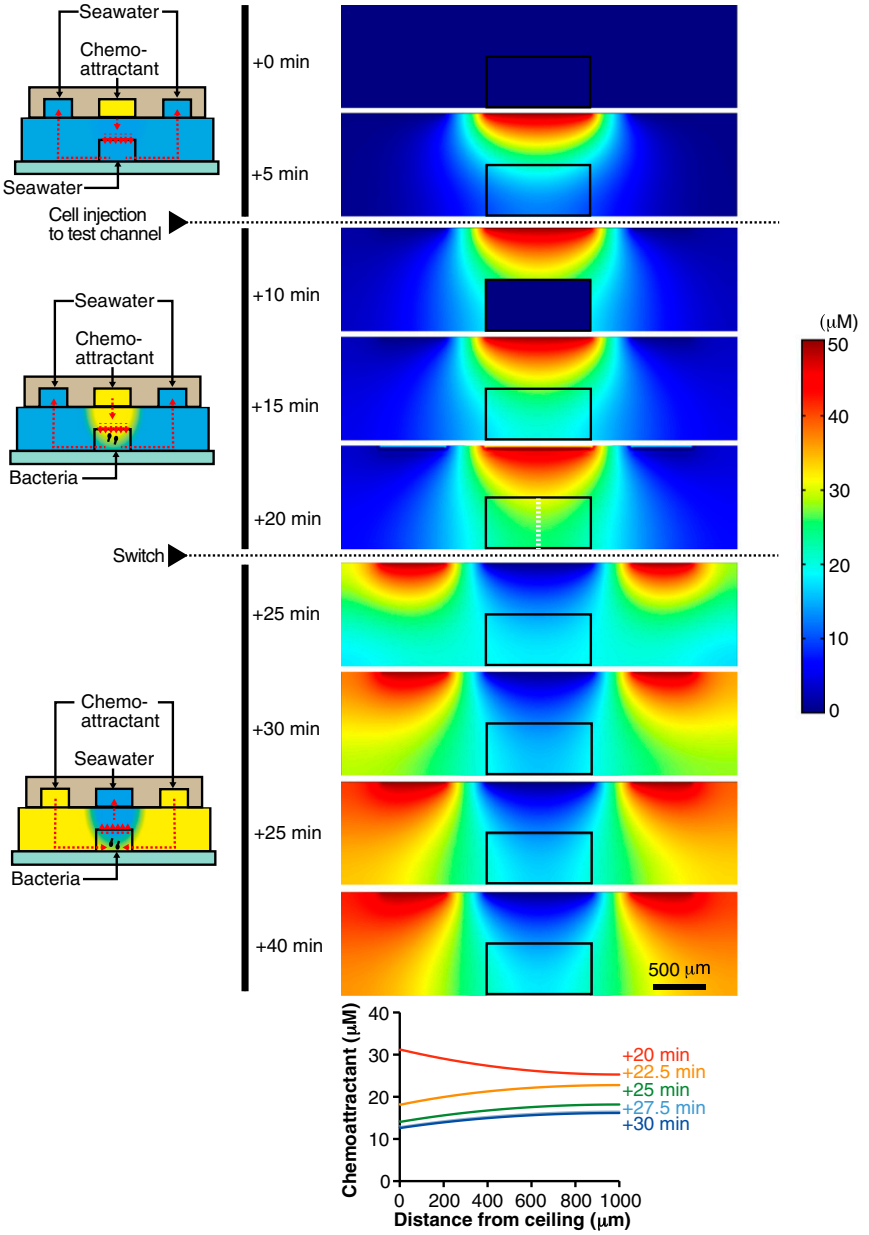

Fig. S6. Temporal evolution of the chemoattractant gradient in the design 3 microdevice (Fig. S5), modeled numerically. Colors represent the chemoattractant concentration (color map) within the agarose layer. Black boxes identify the test channel within the agarose layer in all panels. Different rows correspond to different times, as indicated by the labels on the left. For the first 20 min, the central irrigation channel carried 50 μM chemoattractant and the side irrigation channels carried seawater (0 μM). At 10 min past the initiation of gradient generation, cells were introduced into the test channel. After 20 min, the conditions were swapped: The central irrigation channel carried seawater (0 μM) and the side irrigation channel carried 50 μM chemoattractant. This resulted in rapid reversal of the chemoattractant gradient. (*Lower*) The temporal evolution of the chemoattractant concentration profile along the vertical midline of the test channel (shown as a white dotted line in one of the panels).

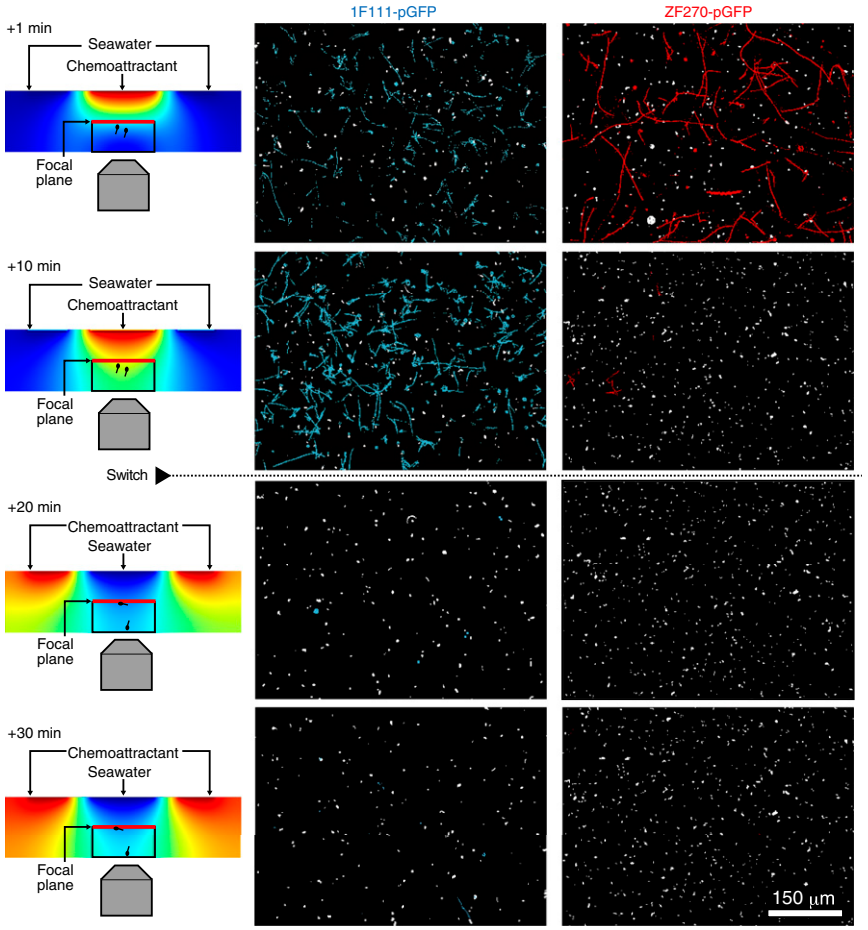

Fig. S7. Cell swimming trajectories directly underneath the agarose ceiling of the design 3 gradient generator device and attachment to that surface. White dots show attached cells imaged by epifluorescence microscopy with a 1-s exposure time. The blue and red overlays show swimming trajectories for the S- and L-population isolates, respectively. The gradient direction was initially upward across the test channel and toward the surface being imaged (Fig. S6), and was reversed 10 min after the inoculation of cells into the test channel (as shown by the schematics; *Left*). Images shown are representative results from three independent experiments.

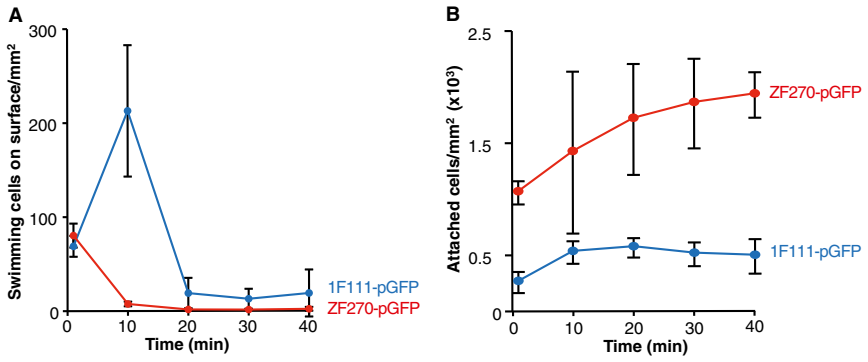

Fig. S8. Time course of cell behavior at the agarose ceiling surface of the design 3 gradient generator device for the experiments shown in Fig. S7. (*A*) Number of cells swimming directly adjacent to the surface (hovering) per unit area. (*B*) Number of cells attached to the surface per unit area. Symbols are averages from three independent experiments, and error bars denote SDs.

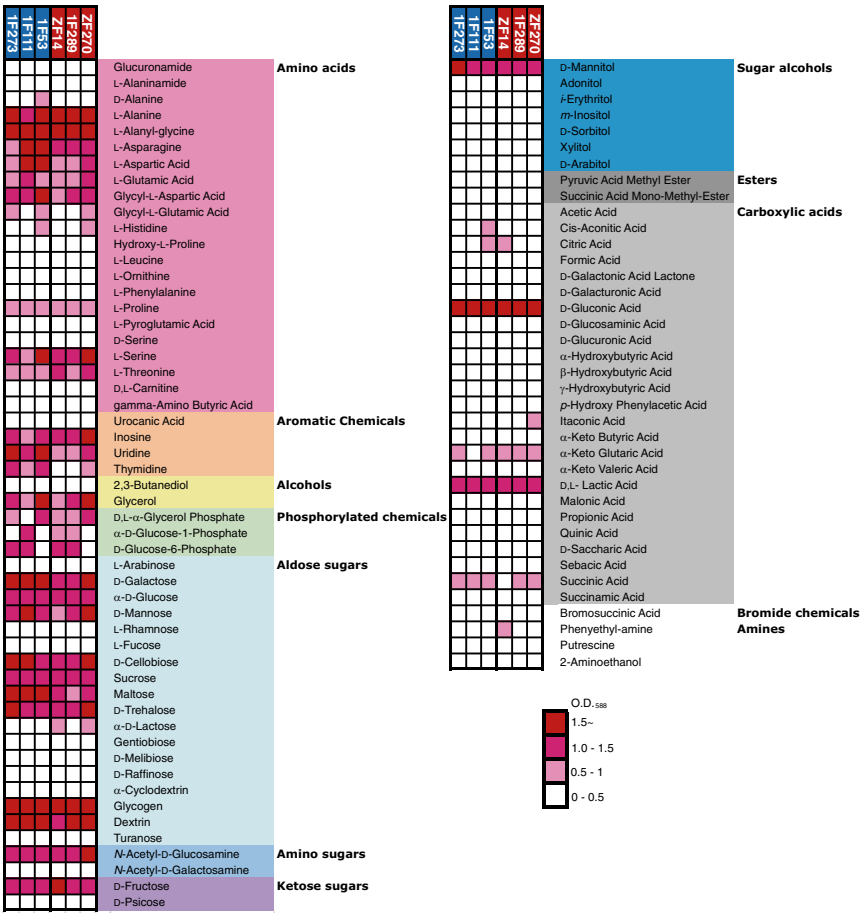

Fig. S9. Substrate utilization by six isolates of *V. cyclitrophicus* measured with a Biolog assay. Three isolates were from the S population (blue) and three were from the L population (red). Colors indicate the relative magnitude of the substrate utilization measured in terms of the OD_{588} (color bar), with white indicating no utilization ($OD_{588} < 0.5$).

Table S1. Isolates of *V. cyclitrophicus* used in this study

Isolates	Population	Size fraction, μm	Notes	Source
1F111	S	1–5	All isolates are from the coast of New England, USA	(1, 2)
1F273	S	1–5		
1F175	S	1–5		
1F53	S	1–5		
1F97	S	1–5		
ZF14	L	>63		
ZF205	L	>63		
ZF270	L	>63		
ZF28	L	>63		
ZF30	L	>63		
ZF65	L	>63		
1F289	L	1–5		
1F111-pGFP	S	1–5	Isolate 1F111 harboring pGFP	This study
ZF270-pGFP	L	>63	Isolate ZF270 harboring pGFP	This study

The pGFP plasmid is a green fluorescent protein-expressing vector and is carrying a spectinomycin resistance gene as a marker (Clontech Laboratories).

1. Shapiro BJ, et al. (2012) Population genomics of early events in the ecological differentiation of bacteria. *Science* 336(6077):48–51.
2. Hunt DE, et al. (2008) Resource partitioning and sympatric differentiation among closely related bacterioplankton. *Science* 320(5879):1081–1085.

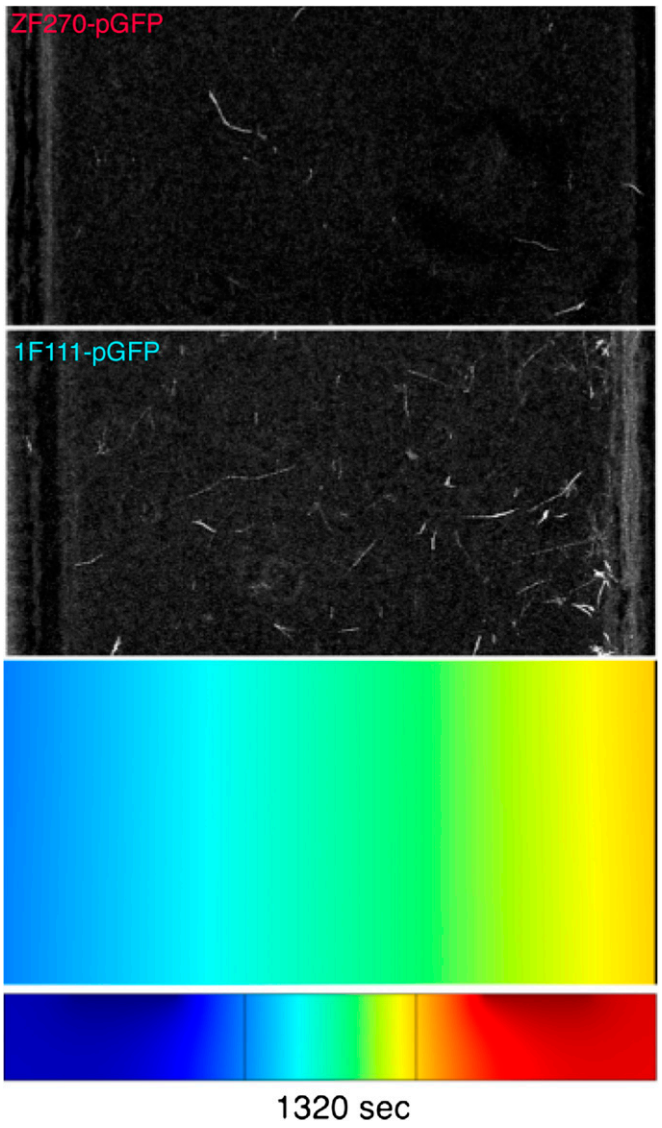

Movie S1. Behavioral response of one S-population isolate (1F111) and one L-population isolate (ZF270) in a temporally varying nutrient landscape. The upper two panels show cell swimming trajectories of 1F111-pGFP (S) or ZF270-pGFP (L) isolates, as indicated. Shown is the vertical (*xy* in Fig. S3) cross-section of the test channel (width 1 mm). Serine release into the test channel occurred from the left sidewall for the first 10 min and was then switched to the right sidewall. The lower two panels show the temporal dynamics of the chemoattractant concentration field in this experiment (design 2; Fig. S3), modeled numerically. Each panel shows the concentration field within the vertical (*xz*) cross-section of the agarose layer and the test channel, as indicated. Colors represent the chemoattractant distribution (see color map in Fig. S4).

Movie S1